Development of Small Designer Aldolase Enzymes: Catalytic Activity, Folding, and Substrate Specificity†

Fujie Tanaka,* Roberta Fuller, and Carlos F. Barbas, III*

The Skaggs Institute for Chemical Biology and Departments of Chemistry and Molecular Biology, The Scripps Research Institute, 10550 North Torrey Pines Road, La Jolla, California 92037

Received February 4, 2005; Revised Manuscript Received March 22, 2005

ABSTRACT: Small (24−35 amino acid residues) peptides that catalyze carbon−carbon bond transformations including aldol, retro-aldol, and Michael reactions in aqueous buffer via an enamine mechanism have been developed. Peptide phage libraries were created by appending six randomized amino acid residues to the C-terminus or to the N-terminus of an 18-mer α-helix peptide containing lysine residues. Reaction-based selection with 1,3-diketones was performed to trap the amino groups of reactive lysine residues that were necessary for the catalysis via an enamine mechanism by formation of stable enaminones. The selected 24-mer peptides catalyzed the reactions with improved activities. The improved activities were correlated with improved folded states of the peptides. The catalyst was then improved with respect to substrate specificity by appending a phage display-derived substrate-binding module. The resulting 35-mer peptide functioned with a significant proportion of the catalytic proficiency of larger protein catalysts. These results indicate that small designer enzymes with good rate acceleration and excellent substrate specificity can be created by combination of design and reaction-based selection from libraries.

Generation of enzyme-like small designer peptide catalysts that achieve the proficiency of natural enzymes with desired substrate specificity is a challenging task. Designer protein catalysts have been prepared by engineering naturally occurring enzymes (*1*−*4*) and by using antibody libraries (i.e., immune diversity) and selection with designed small molecule compounds (*5*−*7*). For experimental purposes, small peptides are more useful and convenient than large proteins, as long as they provide the same function, because small peptides can be more easily prepared and their characterization is simpler. However, fundamental questions remain to be answered: Can small peptides attain the catalytic efficiency of larger protein catalysts, and how can these peptide catalysts best be developed? The folded states of enzymes are key to their catalytic activity since structure can be used productively to modify the chemical reactivity of amino acid side chains. Small peptides are often limited in their potential to catalyze reactions because of the limited ability to adopt well-defined structures. Small peptides have also demonstrated limited specificity for small substrate molecules.

For small catalytic peptides (<50 amino acid residues) that function in aqueous buffer, rational design has been used for the creation of catalysts of the decarboxylation of oxaloacetic acid (*8*−*12*), ester hydrolysis (*13*−*15*), and transesterifications (*13*). Rational design, however, is limited in throughput. A combination of rational design and library-based methods with reaction-based selection, which has been used for the development of antibody catalysts (*7*), may be an attractive approach to small peptide catalyst development (*16*, *17*). Here we have explored strategies for the creation of small designer enzymes. We have developed small peptides that catalyze carbon−carbon bond formation and cleavage via an enamine mechanism. First, reaction-based selection from peptide phage libraries was performed to develop peptides that possessed improved catalytic activity. The peptide was then improved with respect to specificity for a small molecule substrate by appending a phage display-derived substrate-binding domain. To understand key factors critical for catalysis performed by small peptides, we have characterized the peptides with respect to catalysis, folded state, and substrate specificity. This research addresses how small peptides with improved catalytic activity and with improved substrate specificity can be created and how the catalytic activity of small peptides might approach that of larger protein catalysts.

MATERIALS AND METHODS

Construction of the XXXXXXYKLLKELLAKLKWLLRKL Library [(NNK)6-YLK Library]. Oligonucleotides YLK-18opt-SfiI-HindIII-f (5′-CGGCCTACAAGCTTCTGAAGGAACTGCTCGCTAAACTGAAGTGGCTGCTCCGTAAACTGGGCCAGGC-3′) (10 μg) and YLK-18opt-SfiI-HindIII-b (5′-TGGCCCAGTTTACGGAGCAGCCACTTCAGTTTAGCGAGCAGTTCCTTCAGAAGCTTGTAGGCCGCCT-3′) (10 μg) were mixed in a total volume of 40 μL, and the mixture was heated at 95 °C for 2 min and then cooled to 25 °C. This mixture was ligated to *Sfi*I-digested pComb3X to give construct A. Oligonucleotides YLK-18opt-SfiI-f (5′-CGGCCTACAAACTGCTGAAGGAACTGCTCGCTAAACTGAAGTGGCTGCTCCGTAAACTGGGCCAGGC-3′) (10 μg) and

† This study was supported in part by the NIH (Grant CA27489) and The Skaggs Institute for Chemical Biology.

* To whom correspondence should be addressed. C.F.B.: e-mail, carlos@scripps.edu; fax, 858-784-2559; phone, 858-784-9098. F.T.: e-mail, ftanaka@scripps.edu; fax, 858-784-2559; phone, 858-784-2559.

10.1021/bi050216j CCC: $30.25
Published on Web 04/26/2005

YLK-18opt-SfiI-b (5′-TGGCCCAGTTTACGGAGCAGC-CACTTCAGTTTAGCGAGCAGTTCCTTCAGCAGTTT-GTAGGCCGCCT-3′) (10 μg) were mixed in a total volume of 40 μL, and the mixture was heated at 95 °C for 2 min and then cooled to 25 °C. This mixture was ligated to *Sfi*I-digested pComb3X to give construct B. Construct B was used as a template for PCR using primers EcoRI-f (5′-TTTTGAATTCAGGAGGAAATTTAAAAAT-GAAAAAGACAGGAACTATCGCGATTG-CAGTGGCACTG-3′) and HindIII-NNK6-SfiI-b (5′-GAGGAGGA-GAAGCTTGTA-$(MNN)_6$GGCCGCCT-GGGCCACGGT-3′), where M = A or C and N = A, C, G, or T. The PCR conditions were as follows: 1 μg of each primer, 100 ng of the template, 2.5 mM each dNTP, and 2.5 units of Taq polymerase in a total volume of 100 μL, with a program of 94 °C for 30 s; 94 °C for 15 s, 56 °C for 15 s, 72 °C for 1 min (25 times); and 72 °C for 5 min. The PCR product was digested with *Eco*RI−*Hin*dIII, and the digested fragment was ligated to *Eco*RI−*Hin*dIII-digested construct A to give the (NNK)6-YLK library in pComb3X.

Construction of the YKLLKELLAKLKWLLRKLXXXXXX Library [YLK-(NNK)6 Library]. Oligonucleotides YLK18-f (5′-GAGGAGGTGGCCCAGGCGGCCTACAAGCT-TCTGAAGGAACTGCTCGCTAAACTGAAGTGGCTG-CTCCGTAAACTG-3′) (10 μg) and YLK18-NNK6-b [5′-GAGGAGGAGGCCGGCCTGGCC$(MNN)_6$CAGTTTACGG-AGCAGCCA-3′] (10 μg) and 2.5 mM each dNTP were mixed with 10× NEBuffer 1 (New England Biolabs, NEB) (10 μL) and with 10× NEBuffer 2 (NEB) (10 μL) in a total volume of 196 μL, and the mixture was heated at 95 °C for 2 min. After being cooled to 25 °C, 20 units of DNA polymerase I, large (Klenow) (5 units/μL, 4 μL), was added to the mixture. After 15 min at 25 °C, the enzyme was denatured at 75 °C for 20 min. The mixture was EtOH precipitated and digested with *Sfi*I followed by purification using Centri-spin-20 (Princeton Separation). The *Sfi*I-digested fragment was ligated to an *Sfi*I-digested pComb3X to give the YLK-(NNK)6 library in pComb3X.

Binding Selection against Diketone Haptens Using a Phage Display System. The ligation mixture was ethanol precipitated and transformed into *E. coli* ER 2537 cells by electroporation (three transformations per library). After transformation, SOC (2% tryptone, 0.5% yeast extract, 0.05% NaCl, 2.5 mM KCl, 10 mM $MgCl_2$, 20 mM glucose) (5 mL) was immediately added into the each reaction, and the cells were grown at 37 °C. After 1 h, super broth (3% trypton, 2% yeast extract, 1% Mops) (SB) (10 mL) and carbenicillin (50 μg/mL) were added. The library size was determined to be 4.7×10^7 for the (NNK)6-YLK library and 4.6×10^7 for the YLK-(NNK)6 library, respectively, by plating of this stage culture (10, 1.0, and 0.1 μL) onto carbenicillin (100 μg/mL) plates of LB agar (carb plates). After 2 h, helper phage VCS-M13 (7.8×10^{12}) were added, and the three cultures for each library were combined into SB (total volume 150 mL) containing carbenicillin (50 μg/mL). After 2 h, kanamycin (70 μg/mL) was added, and the culture was incubated at 37 °C overnight. The cells were removed by centrifugation (4000 rpm, 30 min), to the supernatant was added poly(ethylene glycol) 8000 [final concentration 4% (w/v)] and NaCl [final concentration 3% (w/v)], and after 30 min on ice, the mixture was centrifuged (9000 rpm, 20 min) (PEG precipitation). The phage precipitate was resuspended in 1% BSA[1]/PBS (10 mM Na_2HPO_4, 1.8 mM KH_2PO_4, 137 mM NaCl, 2.7 mM KCl, pH 7.4) (5.0 mL) and filtered (0.2 μm).

Wells of a microtiter plate (Costar 3690) were coated with **1**−BSA (two wells per library) and **2**−BSA (two wells per library) (3−5 μg/25 μL of PBS per well) at 4 °C overnight, washed with H_2O two times, and blocked with 3% BSA/PBS (170 μL per well) at room temperature for 1.5 h. Blocking solution was removed, and the library phage (25 μL per well) was added. After 2 h, the wells were washed 10 times with 0.5% Tween 20/PBS (PBST) to remove unbound phage, and then the bound phage were eluted by trypsin digestion (Difco trypsin 1:250, 10 mg/mL in TBS, 50 μL per well) at 37 °C for 30 min. The elution was added to *Escherichia coli* ER2537 cells (15 mL in SB). The eluted phage were combined on the basis of the diketones. The culture was incubated at 37 °C. After 15 min, the infected cell culture (30 μL) was diluted with SB (270 μL) and plated (1, 10, and 100 μL) on carb plates to determine the output. Carbenicillin (50 μg/mL) was added to the infected cell culture and shaken at 37 °C for 1 h. Helper phage VCS-M13 (1 mL, 2.6×10^{12} pfu) were added, and the culture was diluted into 100 mL with SB containing carbenicillin (50 μg/mL). After 2 h, kanamycin (70 μg/mL) was added, and the culture was incubated at 37 °C overnight. After centrifugation and PEG precipitation as described above, the phage precipitate was resuspended in 1% BSA/PBS (pH 7.4) (2.0 mL) and filtered (0.2 μm). This phage solution was used for further panning. For the second and third rounds, phage were added to the BSA-coated wells, incubated for 30 min at room temperature to exclude the phage that bound to BSA, and then transferred to hapten-coated wells.

Screening Functional Peptides and Sequence Analysis. After the third round panning, the eluted phage were used to infect *E. coli* ER2537 cells, and the peptide-pIII fusion was used for the ELISA to screen for the clones that produced soluble peptides that bound to the diketones. Individual colonies were picked from the plates and grown in SB (5 mL) containing carbenicillin (50 μg/mL) at 37 °C for 7 h. Expression of the Fab genes was induced by addition of IPTG (1 mM), and the cultures were incubated overnight. The culture was centrifuged (3500 rpm, 20 min), and the supernatant was used for assessing the binding activity by ELISA using **1**− and **2**−BSA. For the screening of soluble peptides (peptide−decapeptide fusions) that bind to the diketones, 20 clones for the library panned with **1**−BSA and 10 clones for the library panned with **2**−BSA were assayed. FT-YLK3 and FT-YLK4 were found in the library panned with **2**−BSA. For the screening of peptide-pIII fusions that bound to the diketones, 20 clones for the library panned with **1**−BSA and 20 clones for library panned with **2**−BSA were assayed. FT-YLK25 was identified from ELISA of peptide-pIII fusion.

The ELISA was performed using the following procedure. Microtiter plates (Costar 3690) were coated with **1**−BSA (0.5 μg/25 μL of PBS per well) at room temperature overnight, washed two times with H_2O, and blocked with 3% BSA/PBS (50 μL per well) at room temperature for 1 h. Blocking solution was removed, the ELISA sample (25 μL

[1] Abbreviations: BSA, bovine serum albumin; ELISA, enzyme-linked immunosorbent assay; ee, enantiomeric excess.

per well) was added, and the plate was incubated at room temperature for 2 h. The well was washed 10 times with H_2O. The bound peptide was detected using alkaline phosphatase conjugated anti-decapeptide antibody and the phosphatase substrate *p*-nitrophenyl phosphate. The resulting yellow color was measured at 405 nm.

The nucleotide sequence of the peptide encoding regions was analyzed using 5′-primer ompseq (5′-AAGACAGCTATCGCGATTGCA-3′).

Peptides. Peptides were synthesized on a peptide synthesizer using standard Fmoc solid-phase peptide synthesis chemistry, were purified by HPLC to >95% purity, and were characterized by electrospray mass spectrometry.

Enaminone Formation (Figure 1). Reactions were initiated by adding 5 μL of 2,4-pentanedione (100 mM in CH_3CN) to 95 μL of peptide solution in a 96-well UV plate (Costar 3635) at 25 °C. The final conditions were [peptide] 100 μM and [2,4-pentanedione] 5 mM in 5% CH_3CN−42.5 mM sodium phosphate buffer (total volume 100 μL). The enaminone formation was measured by following the difference in absorption at 318 nm and at 400 nm for 2 h 40 min using a microplate spectrophotometer.

*Catalytic Assay and Kinetics for Retro-Aldol Reactions of **4** and **5**.* Reactions were initiated by adding 5 μL of a stock solution of substrate **4** or *anti*-**5** in CH_3CN to 95 μL of peptide solution in sodium phosphate buffer (pH 7.5) at 25 °C for a 96-well plate (Costar 3915). The final conditions were [peptide] 100 μM and [substrate] 250 μM−2 mM in 5% CH_3CN−42.5 mM sodium phosphate buffer (pH 7.5) (total volume 100 μL) except where noted. The increase in the fluorescence (λ_{ex} 330 nm, λ_{em} 452 nm) was monitored by using a microplate spectrophotometer. The observed rate was corrected for the uncatalyzed rate in the absence of peptide. The kinetic parameters, k_{cat} and K_m, were determined by curve fitting of S−V plots as described by the Michaelis−Menten equation using MacCurveFit (Kevin Raner).

*Catalytic Assay and Kinetics for Retro-Aldol Reactions of **12**.* The reaction was initiated by adding 8 μL of a stock solution of **12** in CH_3CN to a mixture of 4 μL of 1 mM peptide in H_2O and 68 μL of 50 mM sodium phosphate (pH 7.5) at 25 °C. The formation of the product aldehyde was measured by HPLC with 10 μL injections of the reaction mixture. Analytical HPLC was performed using a Microsorb-MV C18 analytical column (Varian) eluted with 40% CH_3CN−0.1% aqueous trifluoroacetic acid (TFA) at a flow rate of 1.0 mL/min, with detection at 254 nm. The retention time of the product aldehyde was 11 min, and that of **12** was 7.0 min. The initial velocities were determined from the linear range of the rate. Since nearly equal peptide−substrate concentrations were employed in the assay, the k_{cat} and K_m were determined according to the procedure reported by Smith et al. (*18*).

Retro-Aldol Reactions of D*-Erythrose.* Reactions were initiated by adding 8 μL of a stock solution (50 mM) of D-erythrose in H_2O to 72 μL of peptide solution in sodium phosphate buffer (pH 7.5) at 25 °C. The final conditions were [peptide] 50 μM and [D-erythrose] 5 mM in 42.5 mM sodium phosphate buffer (pH 7.5) (total volume 80 μL). To follow the reaction, an aliquot of the reaction (12 μL) was mixed with 1 μL of 250 mM *p*-nitroaniline in MeOH, 1 μL of CH_3COOH, and 1 μL of 2 M $NaBH_3CN$ in H_2O, and after 10 min, the mixture (10 μL) was injected onto HPLC to analyze the product 2-[(4-nitrophenyl)amino]ethanol. The analytical HPLC was performed using a Microsorb-MV C18 analytical column at a flow rate of 1.0 mL/min, with detection at 400 nm. The elution was 8% CH_3CN−0.1% aqueous TFA, and the retention time of 2-[(4-nitrophenyl)amino]ethanol was 17.1 min.

Catalytic Assay for Aldol and Michael Reactions. Reactions were initiated by adding 5 μL of a stock solution of substrate aldehyde in CH_3CN to a mixture (95 μL) of acetone and of peptide solution at 25 °C. The rate of the reaction was measured by HPLC detection of **4**, **9**, or **11** with a 10 μL injection of the reaction mixture. The analytical HPLC was performed using a Microsorb-MV C18 analytical column at a flow rate of 1.0 mL/min, with detection at 254 nm. For the aldol reaction to afford **4**, the elution was 40% CH_3CN−0.1% aqueous TFA, and the retention times of **4** and **7** were 5.6 and 9.6 min, respectively. For the aldol reaction to afford **9**, the elution was 30% CH_3CN−0.1% aqueous TFA, and the retention times of **9** and **8** were 5.4 and 7.0 min, respectively. For the Michael reaction to afford **11**, the elution was 15% CH_3CN−0.1% aqueous TFA, and the retention times of **11** and **10** were 13.4 and 16.3 min, respectively. The enantiomeric excess of **9** was determined by HPLC analysis using a Chiralpak AD-RH (Daicel) column. The elution was 30% CH_3CN−0.1% aqueous TFA, and the retention times of (*R*)- and (*S*)-**9** were 15.0 and 17.9 min, respectively, at a flow rate of 1.0 mL/min with detection at 254 nm.

RESULTS AND DISCUSSION

Mechanism-Based Selection of Peptides. Many carbon−carbon bond formation and cleavage reactions in biological systems proceed through an enamine mechanism (*19*−*22*). Enzymes often use lysine ϵ-amino groups to form an enamine in their catalytic reactions; however, most ϵ-amino groups of lysine residues are not nucleophiles. Special environments within the three-dimensional folded structures of enzymes are required in order for the amino group to act as a nucleophile for enamine formation with carbonyl compounds. To access peptides possessing such reactive residues, reaction-based selection using combinatorial libraries combined with peptide design should be useful. We have recently demonstrated that reaction-based selection using phage display with 1,3-diketones can be used to access antibody catalysts operating via an enamine mechanism (*23*, *24*). The diketones were previously used to modify nucleophilic ϵ-amino groups of lysine residues of enzymes by the formation of enaminones (*25*, *26*). In addition, antibodies that catalyze aldol reactions (aldolase antibodies) via an enamine mechanism were also generated by reactive immunization with 1,3-diketone derivatives (*7*, *27*). Therefore, to develop small peptide catalysts that operate via an enamine mechanism, we have performed reaction-based selection with 1,3-diketones (*28*).

Amine-catalyzed decarboxylation and aldol reactions share imine and enamine intermediates on their reaction coordinates. Accordingly, enzyme and antibody catalysts of these reactions are generally bifunctional catalysts capable of accelerating both decarboxylation and aldol reactions (*29*, *30*). To select peptides that operate via an imine/enamine reaction mechanism, we sought to exploit mechanistic

Scheme 1: Diketones, Enaminone Formation, Modification with *N*-Acyl-*β*-lactam, and Retro-Aldol Reactions

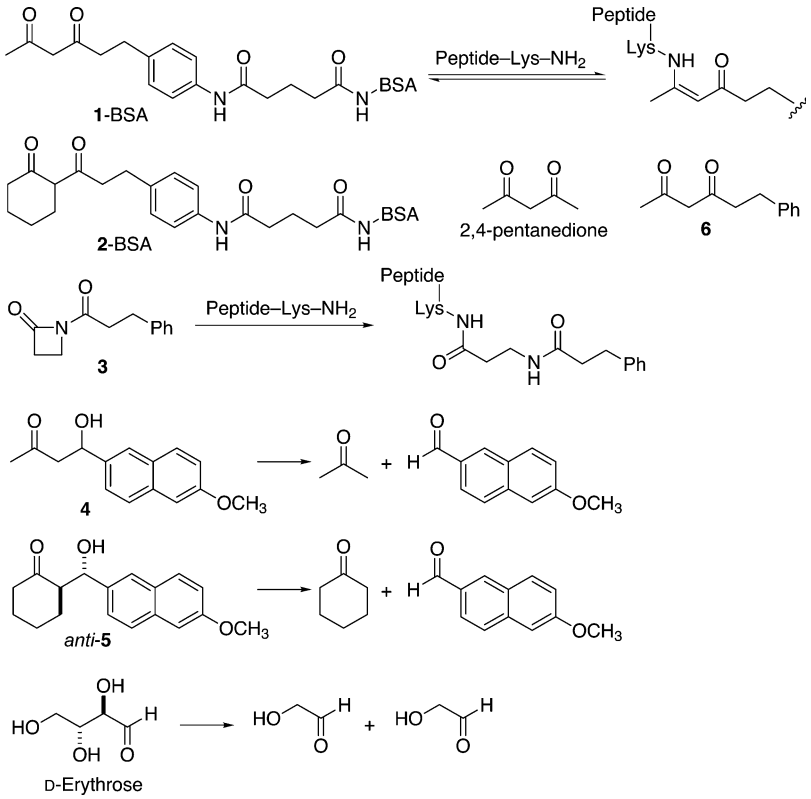

Table 1: Sequences of Peptides

peptide name	sequence (C-terminal amide)
YLK-18opt	YKLLKELLAKLKWLLRKL-NH_2
FT-YLK3	YKLLKELLAKLKWLLRKL**LGPTCL**-NH_2
FT-YLK4	YKLLKELLAKLKWLLRKL**SDHLCL**-NH_2
FT-YLK25	**SPFLGQ**YKLLKELLAKLKWLLRKL-NH_2
FT-YLK3-R5	YRLLRELLARLRWLLRRL**LGPTCL**-NH_2
FT-YLK3-NAc	Ac-YKLLKELLAKLKWLLRKL**LGPTCL**-NH_2
FT-YLK3-23S	YKLLKELLAKLKWLLRKL**LGPTSL**-NH_2
FluS303-FTYLK3	YPNEFDWWDYYYKLLKELLAKLKWLL-RKLLGPTCL-NH_2

homology by using as our starting point an 18-residue peptide (YLK-18opt) (*9*) that catalyzes the decarboxylation of oxalacetic acid. This peptide contains multiple lysine residues that are critical for its activity. To evolve the catalytic activity of this peptide, a six amino acid residue library was appended to the C-terminus or to the N-terminus of the peptide, and the libraries YKLLKELLAKLKWLLRKL**XXXXXX** and **XXXXXX**YKLLKELLAKLKWLLRKL (**X** = any of the natural 20 amino acids) were displayed on phage. Reaction-based selection with 1,3-diketones **1**−BSA (bovine serum albumin) and **2**−BSA was performed from the peptide phage libraries (*31*) to trap the amino groups of reactive lysine residues that were necessary for the catalysis via an enamine mechanism by formation of stable enaminones (Scheme 1).

Enzyme-linked immunosorbent assay (ELISA) was used to identify the clones that bound to **1**− and **2**−BSA from the selected libraries. The three peptides that gave the strongest ELISA signals, FT-YLK3, FT-YLK4, and FT-YLK25, and the parental peptide YLK-18opt were chemically synthesized (C-terminal amide). Peptide sequences are shown in Table 1. Since the solubility of peptide FT-YLK4 was low in aqueous buffer at neutral pH, only FT-YLK3 and FT-YLK25 were characterized.

Enaminone Formation and Reaction with an N-Acyl-β-lactam. The peptides were expected to bind diketones through enaminone formation rather than through noncovalent interactions. The ability of the peptides to form the enaminone was analyzed using 2,4-pentanedione, the smallest compound containing a 1,3-diketone structure. Peptides FT-YLK3, FT-YLK25, and YLK-18opt formed a UV-observable enaminone as monitored at 318 nm (*23*−*28*). The velocities of the enaminone formation of FT-YLK3 and of FT-YLK25 with 2,4-pentanedione were faster than that of YLK-18opt at neutral pH. Selection with diketones afforded peptides with improved rates of enaminone formation compared to the parental peptide. The pH profile of the velocity of the enaminone formation indicated that FT-YLK3 had a pK_a lower than that typical of a lysine ϵ-amino group (pK_a 10.67) (*32*) or an N-terminal amino group, and the lowest pK_a was approximately 5.5 (Figure 1). The selected peptides had neutral amino group(s) at neutral pH that could serve as the nucleopiles for formation of enaminone with the diketones and for catalysis of enamine-based reactions. To provide information about how many of the amino groups of FT-YLK3 were able to form enaminone, i.e., the number of nucleophilic amino groups, the peptide was treated with an *N*-acyl-*β*-lactam derivative **3** at pH 7.5 and analyzed by the MALDI mass spectrometry. Compound **3** was previously used for the selective modification of the enamine-formable nucleophilic lysine ϵ-amino group of aldolase antibodies (*33*). At 30 min, 0−4 additions of **3** per molecule of FT-YLK3 were observed. At 2 h, 1−5 additions, and at 6 h 1−7 additions of **3** per molecule of FT-YLK3 were observed. FT-YLK3 contains tyrosine, threonine, and cysteine residues that can react with **3**. Even with consideration of labeling at these additional modification sites, the results indicated that more than one amino group was labeled per peptide. Any of these

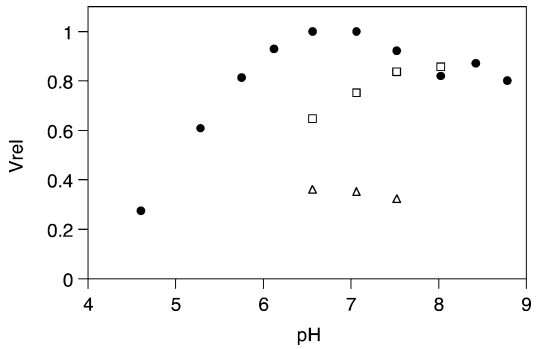

FIGURE 1: Enaminone formation of peptides FT-YLK3 (solid circle), FT-YLK25 (square), and YLK-18opt (triangle) with 2,4-pentanedione. The increase in absorption at 318 nm was monitored in 5% CH_3CN−42.5 mM sodium phosphate at 25 °C, [peptide] 100 μM, and [2,4-pentanedione] 5 mM. The relative velocity (V_{rel}) was compared.

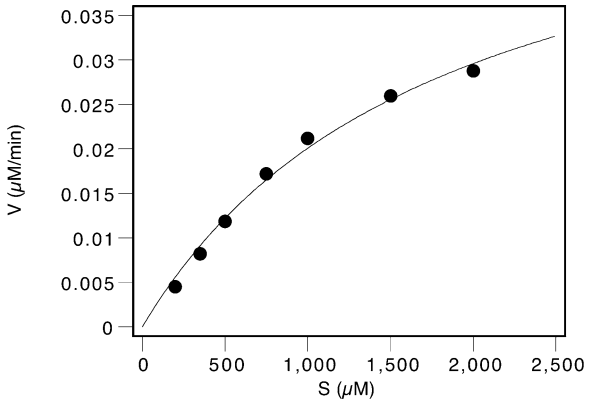

FIGURE 2: S−V plot of the FT-YLK-3-catalyzed retro-aldol reaction of (±)-**4**. Conditions: [FT-YLK3] 100 μM, 5% CH_3CN−42.5 mM sodium phosphate (pH 7.5), and 25 °C.

multiple amino groups could serve as a nucleophile for the enamine-based catalysis. We could not determine the order of the reactivity of the five lysyl residues of the peptide.

Retro-Aldol Reactions. Peptides FT-YLK3 and FT-YLK25 catalyzed the retro-aldol reactions of fluorogenic substrates (±)-**4** and (±)-*anti*-**5** (Scheme 1). FT-YLK3- and FT-YLK25-catalyzed reactions displayed saturation kinetics as described by the Michaelis−Menten equation (Figure 2). The kinetic parameters are shown in Table 2. The K_m values were in the millimolar range. The rate accelerations above the buffer-catalyzed background reaction (k_{cat}/k_{uncat}) of peptides FT-YLK3 and FT-YLK25 were 1400 and 1200 for (±)-**4** and 500 and 250 for (±)-*anti*-**5**, respectively, and were 1.5−3-fold superior to the parental peptide YLK-18opt for the both substrates, respectively.

When diketone **6** (2 mM) was added to a solution of the peptide and then the retro-aldol reaction of **4** was performed, the catalytic activity was inhibited. This result indicates that the binding site for diketones and the catalytic site are shared. Thus, together with the results of enaminone formation with 2,4-pentanedione as described above, these results indicate that these peptides use an enamine mechanism for the retro-aldol reactions.

For a family of aldolase antibodies, a correlation between catalytic activity and reactivity to diketone was observed: Aldolase antibody that catalyzed the retro-aldol reaction with higher activity displayed higher reactivity to the corresponding diketone (*24*). A similar correlation was observed within this family of aldolase peptides (peptides possessing aldolase activity). Peptides FT-YLK3 and FT-YLK25 formed the enaminone with 2,4-pentanedione 2.9- and 2.6-fold faster, respectively, than YLK-18opt at pH 7.5 and catalyzed the retro-aldol reaction of **4** 2.6- and 2.2-fold, respectively, more efficiently based on the k_{cat} than YLK-18opt (Table 2). Improvement in enaminone formation with the diketone correlated with an improved k_{cat} within this family of peptides. Reaction-based selection with diketone provided improved aldolase catalysts that operate via an enamine mechanism.

Lysine ϵ-amino groups of the peptides should be essential for catalysis. To examine the catalytic role of the lysine residues, all five lysine residues in FT-YLK3 were replaced by arginine residues. Peptide FT-YLK3-R5, with five arginines, displayed less than 5% of the catalytic activity of FT-YLK3 when the reaction was performed using peptide (100 μM) and (±)-**4** (2 mM). This result was consistent with the catalytic role for the ϵ-amino groups of the lysine residues of FT-YLK3. To examine the effect of the N-terminal amine, N-terminal acetylated peptide FT-YLK3-NAc was also examined. Peptide FT-YLK3-NAc catalyzed the retro-aldol reaction with the same velocity as that of FT-YLK3, when the reaction was performed by using peptide (100 μM) and (±)-**4** (2 mM). These results indicated that the N-terminal amine of FT-YLK3 was not important for catalysis and lysine ϵ-amino groups were essential for the catalysis.

MALDI mass analysis of FT-YLK3 revealed that the peptide forms a covalent dimer, although a monomer was the main species detected after storage in the reaction buffer used for kinetic studies. The role of the cysteine residue that formed the disulfide bond was assessed by synthesis of the serine analogue FT-YLK3-23S. Peptide FT-YLK3-23S also catalyzed the retro-aldol reaction of (±)-**4**. The velocity of the catalyzed reaction was 75% that of FT-YLK3 when the reaction was performed using peptide (100 μM) and (±)-**4** (2 mM). Thus covalent dimer formation is not essential for catalysis, but dimer formation enhanced the catalytic activity and the folding (see below).

Peptides possessing lysine residue(s), but otherwise not related to YLK-18opt, ELLELDKWASLWNC, ELKDKWASLWNWFNIT, ELDKWASLWNWFDITGGC, and CDEKSKLQEIYQELTQLKAAVGEL, were also analyzed for the retro-aldol reaction of (±)-**4** under the same conditions. Their activities were less than 5% that of FT-YLK3. In addition, 1 mM lysine, arginine, tyrosine, proline, mixtures of these amino acids, or lysyllysine did not catalyze the retro-aldol reactions of **4**.

Studies performed using peptide (100 μM) and each of the enantiomers of **4** (1 mM) in 10% CH_3CN−40 mM sodium phosphate (pH 7.5) revealed that the ratios of the initial velocities of peptide-catalyzed reactions of (*R*)-**4**:(*S*)-**4** were 1.3:1.0 for YLK-18opt, 1.8:1.0 for FT-YLK3, and 1.0:1.0 for FT-YLK25. The selected terminal six residues of the peptides thus had an effect on the enantioselectivity of the peptide-catalyzed reactions. Although the selectivity was moderate, these results indicate that the addition of amino acid sequence can alter substrate specificity.

These peptides also have the potential to catalyze retro-aldol reactions of natural sugars. When a reaction was performed using FT-YLK3 (50 μM) and D-erythrose (5 mM) in 42.5 mM sodium phosphate (pH 7.5), the initial velocity

Table 2: Kinetic Parameters of Peptide-Catalyzed Retro-Aldol Reactions and Relative Velocity of Enaminone Formation

	retro-aldol reaction of (±)-**4**[a]			retro-aldol reaction of (±)-*anti*-**5**[a]			enamine formation with 2,4-pentanedione[b]
peptide	K_m (mM)	k_{cat} (min^{-1})	k_{cat}/k_{uncat}[c]	K_m (mM)	k_{cat} (min^{-1})	k_{cat}/k_{uncat}[c]	V_{rel}
YLK-18opt	1.8	2.1×10^{-4}	540	0.9	4.1×10^{-4}	170	1
FT-YLK3	1.8	5.6×10^{-4}	1400	1.1	1.2×10^{-3}	500	2.9
FT-YLK25	1.8	4.7×10^{-4}	1200	0.9	5.9×10^{-4}	250	2.6

[a] Reaction conditions: [peptide] 100 μM and 5% CH_3CN−42.5 mM sodium phosphate (pH 7.5) for (±)-**4** and 5% DMSO−42.5 mM sodium phosphate (pH 7.5) for (±)-*anti*-**5**, at 25 °C. [b] Conditions: [peptide] 100 μM, [2,4-pentanedione] 5 mM, and 5% CH_3CN−42.5 mM sodium phosphate (pH 7.5). [c] The first-order kinetic constant of the background reaction (k_{uncat}) was 3.9×10^{-7} min^{-1} for (±)-**4** and 2.4×10^{-6} min^{-1} for (±)-*anti*-**5**.

Scheme 2: (a) Peptide-Catalyzed Aldol Reactions and (b) Peptide-Catalyzed Michael Reactions

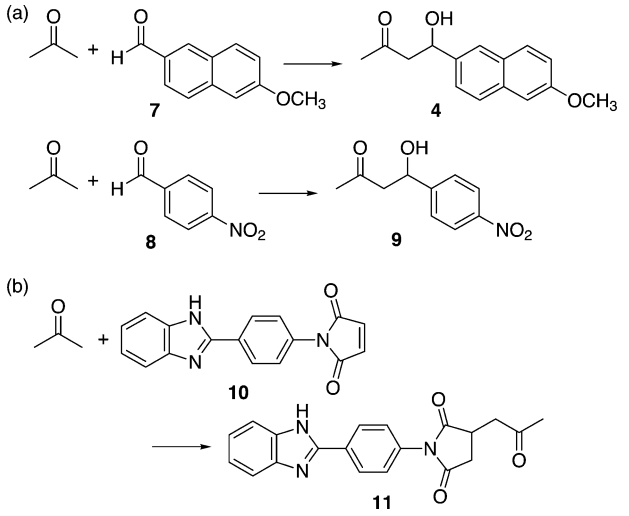

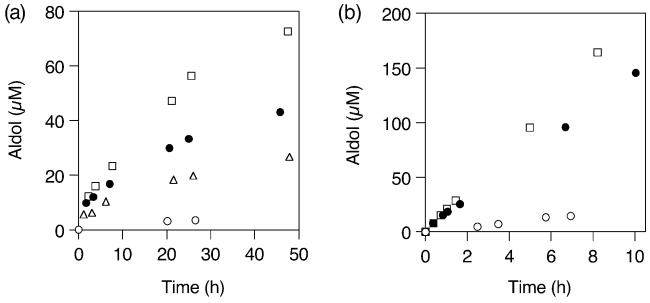

FIGURE 3: Peptide-catalyzed aldol reactions using FT-YLK25 (square), FT-YLK3 (solid circle), YLK-18opt (triangle), and background (open circle). (a) Reaction of acetone and 6-methoxy-2-naphthaldehyde (**7**) to afford aldol **4**. Conditions: [peptide] 100 μM, [acetone] 5% (680 mM), and [**7**] 2 mM in 5% CH_3CN−40 mM sodium phosphate (pH 7.5). (b) Reaction of acetone and 4-nitrobenzaldehyde (**8**) to afford aldol **9**. Conditions: [peptide] 100 μM, [acetone] 5% (680 mM), and [**8**] 2 mM in 5% CH_3CN−42 mM sodium phosphate (pH 7.0).

of the retro-aldol reaction was 3.7×10^{-3} μM/min after background correction (background 5.4×10^{-4} μM/min).

Aldol Reactions. The peptides also catalyzed aldol reactions of acetone and aldehydes (Scheme 2a, Figure 3). The reaction was performed by using peptide (100 μM) and 6-methoxy-2-naphthaldehyde (**7**) (2 mM) in 5% acetone (680 mM)−5% CH_3CN−40 mM sodium phosphate (pH 7.5), and the production of **4** was followed by HPLC assay. The initial velocities of the formation of **4** were 4.6×10^{-2} μM/min for FT-YLK25, 3.3×10^{-2} μM/min for FT-YLK3, and 2.2×10^{-2} μM/min for YLK-18opt after background correction (background 2.3×10^{-3} μM/min) (Figure 3a). The velocities of the peptide FT-YLK25- and FT-YLK3-catalyzed reactions were 20- and 14-fold faster than that of the background and were 2- and 1.5-fold faster than that of YLK-18opt, respectively. The reactions with FT-YLK25 and FT-TLK3 afforded 173 and 110 μM **4** after 14 days, respectively. When the reaction was performed by using peptide (100 μM) and 4-nitrobenzaldehyde (**8**) (2 mM) in 5% acetone (680 mM)−5% CH_3CN−40 mM sodium phosphate (pH 7.0) and the production of **9** was followed by HPLC assay, the initial velocities were 2.9×10^{-1} μM/min for FT-YLK25 and 2.0×10^{-1} μM/min for FT-YLK3 after background correction (background 3.6×10^{-2} μM/min) (Figure 3b). The reactions with FT-YLK25 and FT-TLK3 afforded 488 and 221 μM **9** after 22 h, respectively. Aldol products accumulated to a higher concentration than the peptide catalyst concentration, indicating that the peptides catalyzed the reaction with turnover. The peptide-catalyzed reactions of aldehyde **8** (1 mM) and 1% acetone (136 mM) at pH 7.0 also provided the corresponding aldol product **9**. The initial velocity of the FT-YLK3-catalyzed reaction was 5.4×10^{-2} μM/min (background 3.0×10^{-3} μM/min), and the reaction afforded 190 μM **9** after 72 h. While FT-YLK3 was a slightly better catalyst than FT-YLK25 for the retro-aldol reaction of **4**, peptide FT-YLK25 was a slightly better catalyst than FT-YLK3 for the aldol reaction.

The enantioselectivity of these catalyzed reactions was moderate: the FT-YLK3- and FT-YLK25-catalyzed reaction afforded 10% ee and 8% ee of (*R*)-**9**, respectively, at 7 h after background correction when the reactions were performed under the conditions described in Figure 3b. For FT-YLK3, the (*R*)-configuration of the major product in the aldol reaction was the same as that of the preferred substrate stereochemistry in the retro-aldol reaction. This result was similar to the aldolase antibody-catalyzed reactions: for example, antibody 38C2 catalyzes the retro-aldol reaction of (*S*)-**4** and affords (*S*)-**4** in the aldol reaction (*34*).

Michael Reaction. Since our peptides operate via an enamine mechanism, they should also catalyze other reactions that exploit enamine intermediates. To examine the catalytic breadth of these peptides, the Michael reaction of acetone to maleimide **10** (*35*, *36*) was performed (Scheme 2b). FT-YLK25 and serine mutant FT-YLK3-23S were used for this reaction. When the reaction was performed using peptide (100 μM) and **10** (1 mM) in 5% acetone (680 mM)−2.5% CH_3CN−2.5% DMSO−40 mM sodium phosphate (pH 7.0), the initial velocity of the formation of **11** was 7.6×10^{-2} μM/min for FT-YLK25 and 6.4×10^{-2} μM/min for FT-YLK3−23S (background 3.2×10^{-3} μM/min). The velocities of the peptide-catalyzed reactions were approximately 20-fold faster than that of the background.

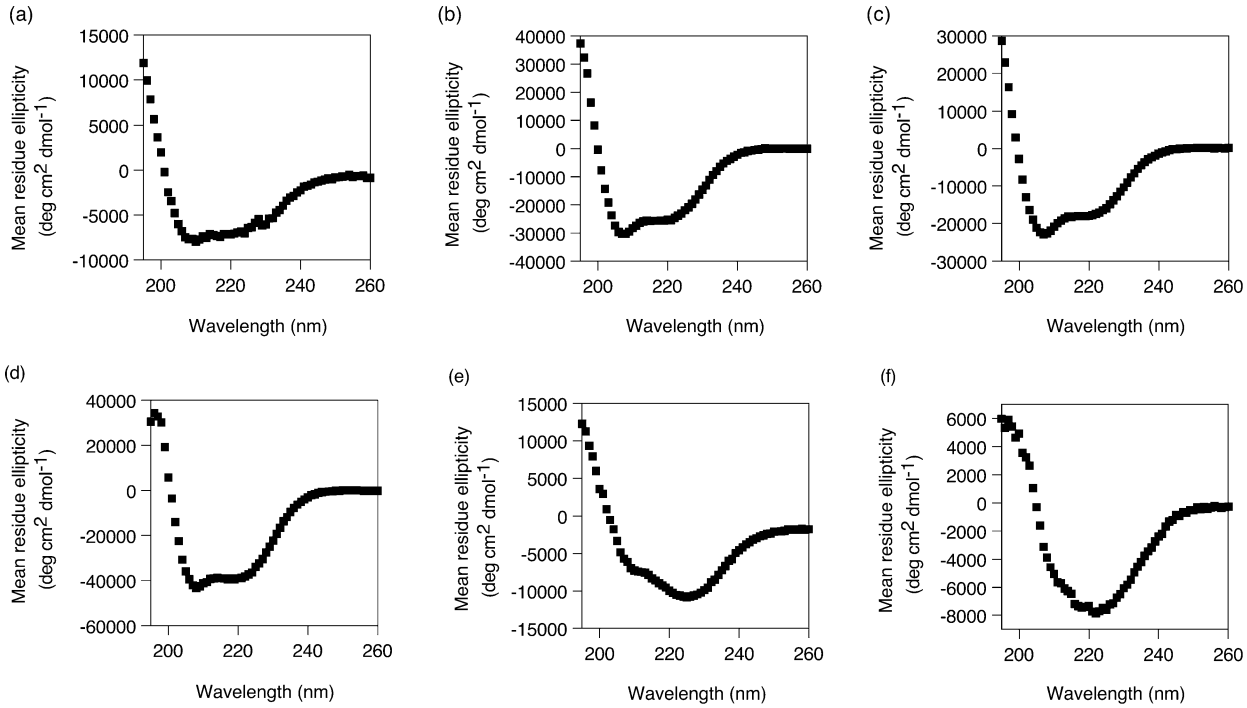

FIGURE 4: CD spectra of peptides: (a) YLK-18opt, (b) FT-YLK3, (c) FT-YLK3-23S, (d) FT-YLK25, (e) FT-YLK3-R25, and (f) FluS303-FTYLK3. The CD spectra were recorded in 45 mM sodium phosphate (pH 7.5) at 25 °C at peptide concentrations of 100 μM, except for FluS303-FTYLK3 which was recorded at 50 μM.

Relationship between Folding and Function. Since no additional amino functionalities were selected in FT-YLK3 and FT-YLK25 compared to YLK-18opt, improvement of the catalytic activity of the peptides may originate from structural changes to the peptide and/or the addition of factors such as acid/base catalysis and transition state stabilization. To analyze the structures of the peptides, circular dichroism (CD) studies were performed. The CD spectra of peptides (100 μM) in 45 mM sodium phosphate buffer (pH 7.5) at 25 °C are shown in Figure 4. For FT-YLK3, the mean residue ellipticities at 208 and 222 nm were -3.04×10^4 and -2.47×10^4 deg cm^2 dmol^{-1}, respectively, and the α-helical content (*37*) was approximately 70% (the mean residue ellipticity of FT-YLK3 was calculated as the monomer). FT-YLK25 also adopted an α-helical structure. The parent peptide YLK-18opt showed a much reduced α-helical content (approximately 20%) under the same conditions. These results suggest that the six amino acid residue extensions stabilize the α-helical conformation of the peptides. The ratio of the mean residue ellipticity of FT-YLK-3-23S at 208 and 222 nm was 0.77, similar to that of FT-YLK3 (0.81). The α-helical content of FT-YLK3-23S was approximately 50%. The retro-aldolase activity of these peptides was correlated with α-helical content (Figure 5). These results indicate that improved catalytic activity is intimately linked with stabilization of the conformation of the peptide. The conformation of the peptides enables their lysine ϵ-amino groups to be more nucleophilic than a lysine in an unstructured environment.

To understand whether the folding was related to self-association, the effect of peptide concentration on function was analyzed. If the peptide functions as a monomer, a linear relationship should be observed in the plot of peptide concentration versus catalytic activity. If self-association of the peptide affects folding and thus catalytic activity, the relationship should be nonliner. Since catalytic activity was correlated to enaminone formation as described above, the velocity of the enaminone formation with 2,4-pentanedione was compared within a series of peptide concentrations. The results showed a nonlinear relationship between the velocity of enaminone formation and peptide concentration (Figure 6). Peptides showed an allosteric-type lag with a slower velocity at a low peptide concentration, although peptides FT-YLK3 and FT-YLK25 began to function at a lower concentration than YLK-18opt. These results indicate that the self-association of peptide molecules is clearly critical to the function of the peptides. The self-association enhanced the appropriate folding of the peptides and vice versa. Addition of six amino acid residues to YLK-18opt improved the folded state of the peptide and thus enhanced the self-association of the peptides and resulted in better function at lower peptide concentrations.

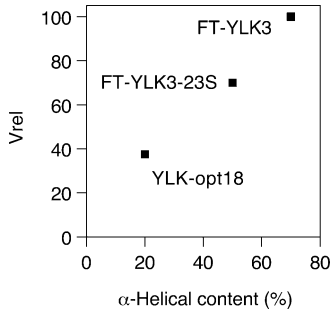

FIGURE 5: Plot of relative velocity (V_{rel}) of the peptide-catalyzed retro-aldol reaction of (±)-**4** versus α-helical content.

Two possible mechanisms for the reactivity change of the lysine ϵ-amino group in proteins have been reported: one involves an electrostatic mechanism (a positively charged residue within an interactive distance of the active site lysine ϵ-amino group acts to modulate the pK_a of a proximal amino

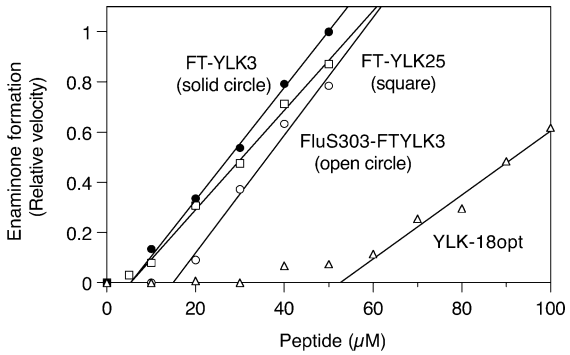

FIGURE 6: Effect of peptide concentration on enaminone formation with 2,4-pentanedione. Conditions: [2,4-pentanedione] 5 mM in 5% CH_3CN−42.5 mM sodium phosphate (pH 7.5). Enaminone formation was monitored at 318 nm. Key: FT-YLK3 (solid circle), FT-YLK25 (square), FluS303−FTYLK3 (open circle), and YLK-18opt (triangle).

group facilitating its reactivity) and the other is the creation of hydrophobic microenvironments (*36*, *38*, *39*). Since the lysine residues of the peptides are within amphipathic α-helical structures and since the self-association and the catalytic activity of the peptides are related, either mechanism or a combination of the both mechanisms would be possible for the peptides described here. It is important to note that the peptides with improved activities and with improved conformational stabilities required for catalysis have been obtained by the reaction-based selection without complicated structural design for the improvement of their catalytic activities.

Improvement of Substrate Specificity and Proficiency of Peptide Catalysts. Although peptides FT-YLK3 and FT-YLK25 showed better catalytic activity than peptide YLK-18opt, the specificity of FT-YLK3 and of FT-YLK25 for the substrates was moderate: their K_m values were in the millimolar range. To improve the substrate specificity, we have developed a modular assembly strategy (*40*). This strategy recruits a substrate-binding module to provide enhanced substrate specificity in covalent combination of binding and catalytic domain modules. When the binding site is in close proximity to the catalytic site, the catalytic site receives the benefit of a higher local substrate concentration provided by sequestering the substrate in close proximity to the catalytic site. The potential advantages of this approach are that it reduces the demand on the functionalization of the catalytic site, which is limited in small peptides, and it is modular, therefore making its adaptation to a variety of specificities rapid.

To endow peptide FT-YLK3 with improved substrate specificity, we sought to covalently connect this peptide to another peptide that binds a substrate molecule with high affinity, anticipating that the local concentration of substrate proximal to the catalytic peptide would be increased. Rozinov and Nolan reported small peptides that bind to small molecule fluorophores (*41*). One of these peptides, YPNEFDW-WDYYY (FluS303 in their paper), binds to fluorescein. This peptide was selected from a combinatorial library of 12-mer peptides displayed on phage. We chose this peptide as our substrate-binding module and attached it to the N-terminus of FT-YLK3. Since FT-YLK3 has a tyrosine residue at the N-terminus and FluS303 has three tyrosine residues at the C-terminus, one tyrosine was removed at the junction.

Chart 1

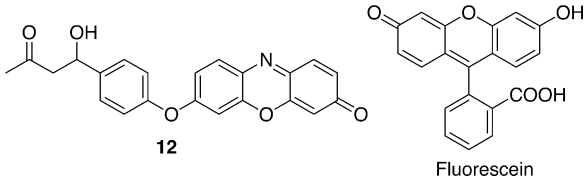

Peptide FluS303-FTYLK3 was chemically synthesized (C-terminal amide) and characterized.

Substrate **12**, which contains a structural moiety from fluorescein, was designed and used in the peptide-catalyzed retro-aldol reactions. The kinetic parameters are shown in Table 3. The K_m value for the FluS303-FTYLK3-catalyzed retro-aldol reaction of substrate **12** was 8 μM, while the K_m of the FluS303-FTYLK3-catalyzed retro-aldol reaction for substrate **4** was 1.1 mM. The K_m value of substrate **12** was 140-fold lower than that of **4** in the FluS303-FTYLK3-catalyzed reaction, and the k_{cat}/K_m value of **12** was 43-fold higher than that of **4**. Thus FluS303-FTYLK3 successfully discriminated between substrates **12** and **4**. As calculated from the K_m values, the differential binding energy ($\Delta\Delta G = -RT \ln\{(K_m \text{ of } \mathbf{12})/(K_m \text{ of } \mathbf{4})\}$ at 25 °C) in favor of substrate **12** over **4** in the FluS303-FTYLK3-catalyzed reactions was 2.9 kcal/mol. The catalytic module itself, FT-YLK3, catalyzed the reaction of **12** with a K_m of 130 μM. Fortuitously, the K_m value of substrate **12** was 14-fold lower than that of substrate **4** in the FT-YLK3-catalyzed reactions. Thus, for FT-YLK3-catalyzed reactions, differential binding of substrate **12** over **4** was favored by 1.6 kcal/mol. Note that the K_m value of FluS303-FTYLK3 with substrate **12** was 16-fold lower than that of FT-YLK3 with **12** while the K_m values of **4** were similar in both the FluS303-FTYLK3- and FT-YLK3-catalyzed reactions. These results indicate that the enhanced substrate specificity of FluS303-FTYLK3 for **12** is the result of two effects. First, binding of **12** to the FT-YLK3 domain as compared to substrate **4** is enhanced by 1.6 kcal/mol. While the exact mechanism for this increase is not clear at present and was not part of the design strategy, heteroatom presentation within **12** may play a role. Second, the addition of the FluS303 sequence to FTYLK3 further increased the affinity of the peptide for substrate **12** ($\Delta\Delta G = 1.7$ kcal/mol) ($\Delta\Delta G = -RT \ln\{(K_m$ of FluS303-FTYLK3-catalyzed reaction of **12**)/(K_m of FT-YLK3-catalyzed reaction of **12**)} at 25 °C) while having a minimal effect on the binding of substrate **4** ($\Delta\Delta G = 0.3$ kcal/mol) ($\Delta\Delta G = -RT \ln\{(K_m$ of FluS303-FTYLK3-catalyzed reaction of **4**)/(K_m of FT-YLK3-catalyzed reaction of **4**)} at 25 °C). We assign this increase in substrate specificity to increase in local substrate concentration at the catalytic site due to the effect of the modular assembly strategy.

Further, when the FluS303-FTYLK3-catalyzed reaction of **12** was performed in the presence of fluorescein (500 μM), the kinetic parameters were K_m 60 μM, k_{cat} 2.5×10^{-4} min^{-1}, and k_{cat}/K_m 4.2 $M^{-1}min^{-1}$. Thus, the K_m value substantially increased while the k_{cat} remained unchanged (within experimental deviation). This result indicates that when fluorescein occupies the substrate-binding domain, in competition with **12**, the specificity constant is greatly reduced. This experiment also validated the modular assembly strategy.

Although the k_{cat} values of peptide catalysts were lower than those of much larger designer protein catalysts such as

Table 3: Kinetic Parameters of Peptide-Catalyzed Retro-Aldol Reactions[a]

peptide	substrate	K_m (μM)	k_{cat} (min^{-1})	k_{cat}/K_m ($M^{-1}\,min^{-1}$)	k_{cat}/k_{uncat}	$(k_{cat}/K_m)/k_{uncat}$ (M^{-1})	$(k_{cat}/K_m)/k_{uncat}$ per residue (M^{-1})
FluS303-FTYLK3	**12**	8	2.3×10^{-4}	29	1800	2.2×10^{8}	6.3×10^{6}
FT-YLK3	**12**	130	2.0×10^{-4}	1.5	1500	1.2×10^{7}	4.9×10^{5}
FluS303-FTYLK3	**4**	1100	7.4×10^{-4}	0.67	1900	1.7×10^{6}	4.9×10^{4}
FT-YLK3[b]	**4**	1800	5.6×10^{-4}	0.31	1400	8.0×10^{5}	3.3×10^{4}

[a] Reaction conditions: [peptide] 50 μM except as noted and 10% CH_3CN−42.5 mM sodium phosphate (pH 7.5) for substrate **12** and 5% CH_3CN−42.5 mM sodium phosphate (pH 7.5) for substrate **4** at 25 °C. [b] [Peptide] 100 μM. See Table 2.

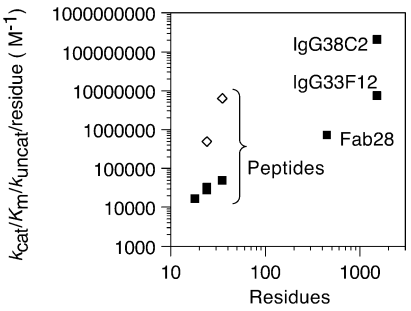

FIGURE 7: Comparison of designer peptide catalysts and antibody catalysts. Plot of $(k_{cat}/K_m)/k_{uncat}$ per residue versus number of amino acid residues found in the peptides and antibody catalysts. Peptides are YLK-opt18, FT-YLK3, FT-YLK25, and FluS303−FTYLK3. For aldolase antibodies IgG38C2, IgG33F12, and Fab28, see ref *24*. Key: substrate **4** (solid squares) and substrate **12** (diamonds).

aldolase antibodies, the catalytic proficiency (*42*) per residue ($(k_{cat}/K_m)/k_{uncat}$ per residue) of the FluS303-FTYLK3-catalyzed reaction of **12** was in the range of those of larger protein catalysts (Figure 7). Peptide FluS303-FTYLK3, which consists of only 35 amino acid residues, had a catalytic proficiency per residue of $6 \times 10^6\ M^{-1}$ (Table 3). This value was comparable to those of antibody catalysts (approximately 1500 and 500 amino acid residues as IgG and Fab form, respectively) on a per residue basis. Some natural enzymes also have catalytic proficiency per residue of approximately $10^6\ M^{-1}$ (*42*). Thus, the 35-mer peptide FluS303-FTYLK3 functioned at near the catalytic proficiency per residue observed for some larger protein catalysts.

FluS303-FTYLK3 also formed a UV-observable enaminone upon addition of 2,4-pentanedione. As indicated in Figure 6, FluS303-FTYLK3 also showed a nonlinear relationship between the enaminone formation velocity and peptide concentration. The concentration necessary to function was approximately 15 μM for FluS303-FTYLK3, similar to that of FT-YLK3 (approximately 5 μM). Appending the substrate-binding domain to FTYLK3 did not affect the function of the catalytic domain. The CD spectra of FluS303-FTYLK3 (50 μM) in 45 mM sodium phosphate (pH 7.5) at 25 °C indicated that the peptide contained α-helical and β-sheet structures (Figure 4f). Studies using the program k2d (*43*) indicate the α-helical content was 27% (maximum error 22.7%). Since the α-helical content of FT-YLK3 (100 μM) was estimated to be approximately 70%, the ideal α-helical content of FluS303-FTYLK3 was calculated to be 48% (24 residues × 0.7/35 residues). Denaturation of the α-helical structure (4.5 M guanidine hydrochloride) as observed in the CD spectra was accompanied by complete loss of catalytic activity. Therefore, with peptide FluS303-FTYLK3, the α-helical structure also correlated with the function.

We have developed small peptides that catalyze carbon−carbon bond formation and cleavage via an enamine mechanism. The reaction-based selection with designed compounds afforded improved small peptide catalysts with respect to both catalytic activity and folded state. We have demonstrated that the reaction-based selection using phage display libraries, which has been effectively used to generate larger protein catalysts (*23*, *24*, *44*), is useful for the development of small designer peptide catalysts. We have also demonstrated that the substrate specificity of the peptide catalyst for a small molecule substrate can be improved by a modular assembly strategy, i.e., covalent conjugation of a binding domain to the catalytic peptide module. We conclude that the combination of design and reaction-based selection from libraries effectively provides small designer enzymes with good rate acceleration and excellent substrate specificity.

REFERENCES

1. Reetz, M. T. (2004) Controlling the enantioselectivity of enzymes by directed evolution: practical and theoretical ramifications, *Proc. Natl. Acad. Sci. U.S.A. 101*, 5716−5722.
2. Joerger, A. C., Mayer, S., and Fersht, A. R. (2003) Mimicking natural evolution in vitro: An *N*-acetylneuraminate lyase mutant with an increased dihydrodipicolinate synthase activity, *Proc. Natl. Acad. Sci. U.S.A. 100*, 5694−5699.
3. Seebeck, F. P., and Hilvert, D. (2003) Conversion of a PLP-dependent racemase into an aldolase by a single active site mutation, *J. Am. Chem. Soc. 125*, 10158−10159.
4. Dwyer, M. A., Looger, L. L., and Hellinga, H. W. (2004) Computational design of a biologically active enzyme, *Science 304*, 196−197.
5. Xu, Y., Yamamoto, N., and Janda, K. (2004) Catalytic antibodies: hapten design strategies and screening methods, *Bioorg. Med. Chem. 12*, 5247−5268.
6. Tanaka F. (2002) Catalytic antibodies as designer proteases and esterases, *Chem. Rev. 102*, 4885−4906.
7. Tanaka, F., and Barbas, C. F., III (2002) Reactive immunization: a unique approach to catalytic antibodies, *J. Immunol. Methods 269*, 67−79.
8. Johnsson, K., Allemann, R. K., Widmer, H., and Benner, S. A. (1993) Synthesis, structure and activity of artificial, rationally designed catalytic polypeptides, *Nature 365*, 530−532.
9. Perez-Paya, E., Houghten, R. A., and Blondell, S. E. (1996) Functionalized protein-like structures from conformationlly defined synthetic combinatorial libraries, *J. Biol. Chem. 271*, 4120−4126.
10. Allert, M., Kjellstrand, M., Broo, K., Nilsson, A., and Baltzer, L. (1998) A designed folded polypeptide model system that catalyzes the decarboxylation of oxaloacetate, *J. Chem. Soc., Perkin Trans. 2*, 2271−2274.
11. Allert, M., and Baltzer, L. (2002) Setting the stage for new catalytic functions in designed proteins−Exploring the imine pathway in the efficient decarboxylation of oxaloacetate by an Arg ± Lys site in a four-helix bundle protein scaffold, *Chem. Eur. J. 8*, 2549−2560.
12. Weston, C. J., Cureton, C. H., Calvert, M. J., Smart, O. S., and Allemann, R. K. (2004) A stable miniature protein with oxaloacetate decarboxylase activity, *ChemBioChem 5*, 1075−1080.
13. Broo, K., Brive, L., Ahlberg, P., and Baltzer, L. (1997) Catalysis of hydrolysis and transesterification reactions of *p*-nitrophenyl esters by a designed helix-loop-helix dimer, *J. Am. Chem. Soc. 119*, 11362−11372.
14. Nilsson, J., and Baltzer, L. (2000) Reactive-site design in folded-polypeptide catalysts−the leaving group pK_a of reactive esters sets

the stage for cooperativity in nucleophilic and general-acid catalysis, *Chem. Eur. J. 6*, 2214−2220.
15. Douat-Casassus, C., Darbre, T., and Reymond, J.-L. (2004) Selective catalysis with peptide dendrimers, *J. Am. Chem. Soc. 126*, 7817−7816.
16. Wei, Y., and Hecht, M. H. (2004) Enzyme-like proteins from an unselected library of designed amino acid sequences, *Protein Eng. Des. Sel. 17*, 67−75.
17. Rutledge, S. E., Volkman, H. M., and Schepartz, A. (2003) Molecular recognition of protein surfaces: high affinity ligands for the CBP KIX domain, *J. Am. Chem. Soc. 125*, 14336−14336.
18. Smith, G. D., Eisenthal, R., and Harrison, R. (1977) Determination of dissociation and Michaelis constants at near-equal enzyme−substrate concentrations, *Anal. Biochem. 79*, 643−647.
19. Heine, A., DeSantis, G., Luz, J. G., Mitchell, M., Wong, C. H., and Wilson, I. A. (2001) Observation of covalent intermediates in an enzyme mechanism at atomic resolution, *Science 294*, 369−374.
20. Allard, J., Grochulski, P., and Sygusch, J. (2001) Covalent intermediate trapped in 2-keto-3-deoxy-6-phosphogluconate (KDPG) aldolase structure at 1.95-Å resolution, *Proc. Natl. Acad. Sci. U.S.A. 98*, 3679−3684.
21. Choi, K. H., Shi, J., Hopkins, C. E., Tolan, D. R., and Allen, K. N. (2001) Snapshots of catalysis: the structure of fructose-1,6-(bis)phosphate aldolase covalently bound to the substrate dihydroxyacetone phosphate, *Biochemistry 40*, 13868−13875.
22. Littlechild, J. A., and Watson, H. C. (1993) A data-based reaction mechanism for type I fructose bisphosphate aldolase, *Trends Biochem. Sci. 18*, 36−39.
23. Tanaka, F., Lerner, R. A., and Barbas, C. F., III (2000) Reconstructing aldolase antibodies to alter their substrate specificity and turnover, *J. Am. Chem. Soc. 122*, 4835−4836.
24. Tanaka, F., Fuller, R., Shim, H., Lerner, R. A., and Barbas, C. F., III (2004) Evolution of aldolase antibodies in vitro: correlation of catalytic activity and reaction-based selection, *J. Mol. Biol. 335*, 1007−1018.
25. Gilbert, H. F., III, and O'Leary, M. H. (1975) Modification of arginine and lysine in proteins, *Biochemistry 14*, 5194−5199.
26. Otwell, H. B., Cipollo, K. L., and Dunlap, R. B. (1979) Modification of lysyl residues of dihydrofolate reductase with 2,4-pentanedione, *Biochim. Biophys. Acta 568*, 297−306.
27. Wagner, J., Lerner, R. A., and Barbas, C. F., III (1995) Efficient aldolase catalytic antibodies that use the enamine mechanism of natural enzymes. *Science 270*, 1797−1800.
28. Tanaka, F., and Barbas, C. F., III (2001) Phage display selection of peptides possessing aldolase activity, *Chem. Commun.*, 769−770.
29. Vlahos, C, J., and Dekker, E. E. (1986) Amino acid sequence of the pyruvate and the glyoxylate active-site lysine peptide of *Escherichia coli* 2-keto-4-hydroxyglutarate aldolase, *J. Biol. Chem. 261*, 11049−11055.
30. Bjornestedt, R., Zhong, G., Lerner, R. A., and Barbas, C. F., III (1996) Copying nature's mechanism for the decarboxylation of β-keto acid into catalytic antibodies by reactive immunization, *J. Am. Chem. Soc. 118*, 11720−11724.
31. Barbas, C. F., III, Burton, D. R., Scott, J. K., and Silverman, G. J., Eds. (2001) *Phage Display: A Laboratory Manual*, Cold Spring Harbor Laboratory Press, Cold Spring Harbor, NY.
32. Lide, D. R., Ed. (2002) *CRC Handbook of Chemistry and Physics*, 83rd ed., p 7-1, CRC Press, New York.
33. Tanaka, F., Lerner, R. A., and Barbas, C. F., III (1999) Thiazolium-dependent catalytic antibodies produced using a covalent modification strategy, *Chem. Commun.*, 1383−1384.
34. Zhu, X., Tanaka, F., Hu, Y., Heine, A., Fuller, R., Zhong, G., Olson, A. J., Lerner, R. A., Barbas, C. F., III, and Wilson, I. A. (2004) The origin of enantioselectivity in aldolase antibodies: crystal structure, site-directed mutagenesis, and computational analysis, *J. Mol. Biol. 343*, 1269−1280.
35. Tanaka, F., Thayumanavan, R., and Barbas, C. F., III (2003) Fluorescent detection of carbon−carbon bond formation, *J. Am. Chem. Soc. 125*, 8523−8528.
36. Tanaka, F., Thayumanavan, R., Mase, N., and Barbas, C. F., III (2004) Rapid analysis of solvent effects on enamine formation by fluorescence: how might enzymes facilitate enamine chemistry with primary amines?, *Tetrahedron Lett. 45*, 325−328.
37. Korsgren, P., Ahlberg, P., and Baltzer, L. (2000) Covalent control of polypeptide folding. Induction of helix-loop-helix motifs by bridging, *J. Chem. Soc., Perkin Trans. 2*, 643−647.
38. Barbas, C. F., III, Heine, A., Zhong, G., Hoffmann, T., Gramatikova, S., Bjornestsdt, R., List, B., Anderson, J., Stura, E. A., Wilson, I. A., and Lerner, R. A. (1997) Immune versus natural selection: Antibody aldolases with enzymic rates but broader scope, *Science 278*, 2085.
39. Westheimer, F. H. (1995) Coincidences, decarboxylation, and electrostatic effects, *Tetrahedron 51*, 3.
40. Tanaka, F., and Barbas, C. F., III (2002) A modular assembly strategy for improving the substrate specificity of small catalytic peptides, *J. Am. Chem. Soc. 124*, 3510−3511.
41. Rozinov, M. N., and Nolan, G. P. (1998) Evolution of peptides that modulate the spectral qualities of bound, small-molecule fluorophores, *Chem. Biol. 5*, 713−728.
42. Radzicka, A., and Wolfenden, R. (1995) A proficient enzyme, *Science 267*, 90−93.
43. Andrate, N., Chacon, P., Merelo, J. J., and Moran, F. (1993) Evolution of secondary structure of proteins from UV circular dichroism spectra using an unsupervised learning neural network, *Protein Eng. 6*, 383−390.
44. Cesaro-Tadic, S., Lagos, D., Honegger, A., Rickard, J. H., Partridge, L. J., Blackburn, G. M., and Pluckthun, A. (2003) Turnover-based in vitro selection and evolution of biocatalysts from a fully synthetic antibody library, *Nat. Biotechnol. 21*, 679−685.

BI050216J